

****Volume Title****

*ASP Conference Series, Vol. **Volume Number***

****Author****

© ****Copyright Year**** *Astronomical Society of the Pacific*

Properties of hot subdwarfs in the *GALEX* survey

P. Nemeth, A. Kawka and S. Vennes

Astronomický ústav AV ČR, CZ-25165 Ondřejov, Czech Republic

Abstract. We have analyzed a sample of hot subdwarfs (sdB, sdO) selected from the *GALEX* ultraviolet sky survey. Applying a model atmosphere analysis we determined the temperature, surface gravity, and helium-to-hydrogen abundance ratio, and obtained preliminary constraints on the CNO abundance for a sample of 181 stars. Adopting colourimetric (ultraviolet-infrared) and quantitative spectral decomposition we also investigated the incidence of solar type or earlier (A, F, G) companions.

1. Introduction

Hot subdwarfs are core He burning stars located at the blue end of the horizontal branch (HB) or extreme horizontal branch (EHB). These subluminoous objects are just below the early-type main-sequence (MS) stars in the Hertzsprung-Russell diagram (HRD). Being in a relatively long lasting (~ 160 Myr) intermediate evolutionary stage of $\sim 1M_{\odot}$ stars they are quite common and are the primary sources of the UV excess of elliptical galaxies, and overwhelm white dwarfs in blue and UV surveys of old stellar populations.

To look for bright, thus nearby white dwarf candidates in the *GALEX* database, Vennes et al. (2011a) devised a method based on UV, optical and infrared colour criteria and sorted out ~ 200 bright ($N_{UV} < 14$) and hot stars. Between 2008 and 2011, systematic, low-resolution spectroscopic follow-up with the ESO/NTT and NOAO/Mayall telescopes confirmed 167 stars as hot subdwarfs. Here, we present the results of a model atmosphere analysis of 127 sdB and 40 sdO stars. Such large and homogeneously modelled samples of bright subdwarfs are useful in identifying candidates for pulsation (e.g., Østensen et al. 2010) and radial velocity studies (e.g., Geier et al. 2011).

2. Spectral fitting

We computed H/He/CNO non-LTE model atmospheres with TLUSTY 200 and synthetic spectra with SYNSPEC 48 (Hubeny & Lanz 1995; Lanz & Hubeny 1995). Model atoms of HI, HeI–II, CII–IV, NIII–V and OIV–VI; and detailed line profiles of H and He were used in SYNSPEC. For all elements, we included at least three model atoms from the OSTAR (Lanz et al. 2003) and BSTAR (Lanz et al. 2007) databases. Model atmospheres for blue horizontal branch stars (BHB) with effective temperatures below 20000 K were calculated with HI, HeI–II, CII–IV, NII–IV and OII–III model atoms. A line list compiled from Kurucz CD-ROM 23 available at the SYNSPEC web page was used.

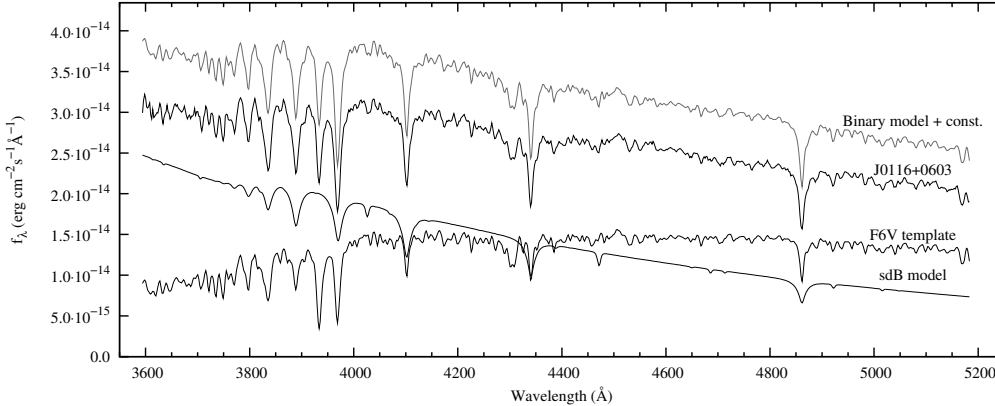


Figure 1. Spectral decomposition of the sdB-F6V binary GALEX J0116+0603.

Spectral fitting was carried out with a combination of the steepest-descent and simplex algorithms implemented in our new χ^2 minimizing fitting program XTGRID. This program written in Python is an adjustable interface for TLUSTY and SYNSPEC designed for iterative multi-wavelength spectral analysis of hot stars from soft X-rays to near infrared wavelengths. The program requires a starting model and with successive adjustments approaches the observed spectrum. Quantitative binary spectral decomposition is also included in XTGRID. Figure 1 shows an example of a fit with binary decomposition for the sdB-F6V binary GALEX J0116+0603.

In general, temperature and gravity have a higher convergence rate than abundances. To take advantage of this property in accelerating our procedure, these parameters can be relaxed (kept fixed for five iterations) after their relative changes decrease below 0.5%. XTGRID is scalable for cluster calculation, and to further accelerate the fitting procedure, previously calculated models are reused until relative changes of temperature and gravity drop below 13% of their respective maximum. Such accelerations are necessary to cope with the computing demand of batch model atmosphere analyses.

After fitting is done, parameter errors for 60, 90 and 99% confidence intervals are estimated by mapping the $\Delta\chi^2$ with respect to the final abundance (X) at representative points in the range of $-0.99 < \delta X/X < 100$. Temperature and gravity errors are measured similarly in the range of $-0.26 < \delta T/T < 0.26$ and $-0.195 < \delta \log g / \log g < 0.195$. Parameters are changed until the statistical limit for 60 % confidence at the given number of free parameters is reached. Then, errors for 90 and 99 % confidence are extrapolated independently by parabolic fits for the upper and lower error intervals. In the final step, L^AT_EX fit summaries and Gnuplot scripts are produced.

For all subdwarfs we applied the initial model with: $T_{\text{eff}} = 40000$ K, $\log g = 5.6$ cm/s^2 , $\log(n\text{He}/n\text{H}) = -1$ and $\log(n\text{CNO}/n\text{H}) = -2$. The maximum relative changes were limited to $\pm 5\%$ (T_{eff}), $\pm 2\%$ ($\log g$); and $+100\%$, -50% for abundances in order to maintain stable TLUSTY convergence. Fitting was continued until relative changes dropped below 0.5% for all parameters in three consecutive iterations. To ignore the low-order variations of the fluxed spectra, our data was sampled in 80 Å sections (each having six to 16 resolution elements depending on the resolution) using the entire spectral range. In order to decrease model atmosphere calculation time we used 30 depth points. Our tests showed this simplification affects model convergence before it would

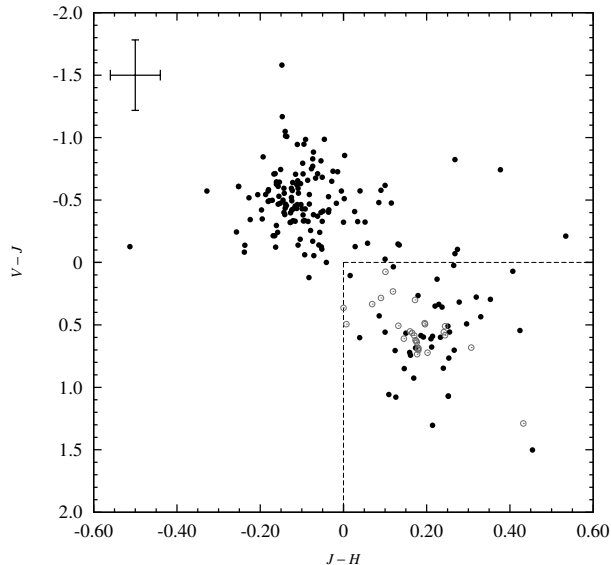


Figure 2. $V-J$ vs. $J-H$ colour-colour diagram for our subdwarf sample. Optical magnitudes were collected from GSC 2.3.2 and infrared from the 2MASS database using VizieR. Apparently single stars aggregate near $V-J \approx -0.5$ and $J-H \approx -0.15$, while composite-spectra binaries show infrared excess (lower right corner). About 19% of the stars have $V-J > 0$ and $J-H > 0$. Open circles show synthetic colour indices of the 27 binaries resolved in this work. Typical errors on photometric colour indices are shown in the upper left corner.

significantly change the emergent flux at low resolution. Model atmospheres were calculated in NLTE radiative equilibrium without convection. Detailed profiles of H and He lines were included, but rotational broadening was not. Modelling of ~ 200 spectra took ~ 800 hours with 6 processors (15.2 GHz total) and required the calculation of about 25000 model atmospheres.

3. Binary decomposition

Binarity is an important aspect of the theory of subdwarf formation and evolution. About 40% of subdwarfs were found in binaries in the SPY sample (Napiwotzki et al. 2004). About half of the subdwarfs show signs of binarity either by having composite spectra, radial velocity variations or spectral signatures (Ca H&K, Fe G band or MgI lines) of a cool companion. Reed et al. (2004) derived a $53 \pm 6\%$ sdB-MS binary fraction from 2MASS $J-H$ and optical $B-V$ colours. Two stars (GALEX J0321+4727 and J2349+3844) from our sample have already been confirmed to be close sdB-MS or WD binaries (Kawka et al. 2010) and GALEX J1717+6757 proved to be an extremely low mass white dwarf-WD binary (Vennes et al. 2011b) based on radial velocity measurements. Further spectroscopic and photometric follow-up should reveal other similar binaries.

A significant number of subdwarfs that were found in composite spectra binaries have challenged model atmosphere analyses as the stellar components need to be reliably separated. These stars were often omitted from surveys due to complications in

carrying out this task. In our sample composite spectra of binaries represent at least 27 objects, or 16% of the sample. This is in accordance with colour measurements (Figure 2), where about 19% of stars show significant IR excess with $V-J > 0$ and $J-H > 0$.

In double-lined binaries both components can be examined simultaneously. Although stellar parameters can be determined with larger errors in these binaries, their analysis is an important task. We built a library of empirical template spectra from the MILES (Cenarro et al. 2007) database to characterize the cool components. Altogether, 946 spectra were included in our library from 3525 to 7500 Å. The best fitting secondary spectrum was searched by interpolating in temperature, surface gravity and metallicity along with TLUSTY model parameters for the primary. In the first step only spectral lines were considered to select an approximate template spectrum, and from the second iteration both the template and the flux ratio of the components were updated. We consider our semi-empirical approach less ambiguous than working with synthetic spectra for both components.

Our method worked well for binaries with late type (F, G) companions, where components have distinct spectral features and comparable optical brightness. We found 21 F and 4 G type MS companions. We also recovered subdwarf-AIII and GIII binaries, but we did not find a significant fraction of A or earlier type companions predicted by population synthesis (Han et al. 2003). However, proper decomposition of such binaries would require UV–optical observations to fit both components.

4. Subdwarf atmospheric parameters

Systematic shifts arise when data from different instruments are modelled with various model atmosphere codes and assumptions. Our sample is large enough and free of such major systematics, therefore appropriate to revisit the distribution of stars in the $T_{\text{eff}}-\log g$ and $T_{\text{eff}}-\text{He}$ planes and to look for possible correlations between surface temperature, gravity and He abundance. The $T_{\text{eff}}-\log g$ diagram is a very important tool in tracking subdwarf evolution, pulsation modes and testing population synthesis predictions.

Out of the 181 stars, we found 127 sdB and 40 sdO stars. This number ratio of ~ 3.2 is close to the previously determined 3 (Heber 2009). We found five He-sdB (or $\sim 4\%$) among the 127 sdBs and 23 He-sdOs (or $\sim 57\%$) out of the 40 sdO stars. Of the 27 resolved binaries only four have sdO primaries.

4.1. The $T_{\text{eff}} - \log g$ plane

Figure 3 shows our GALEX sample in the $T_{\text{eff}} - \log g$ plane. The distribution of stars follow the theoretical EHB and He main-sequence (HeMS), with some stars along post-EHB evolutionary tracks. Grey full lines show the theoretical evolutionary tracks from Dorman et al. (1993) for stellar masses from top to bottom: 0.480, 0.475, 0.473 and 0.471 M_{\odot} . Line widths are proportional to evolutionary time scales. The ZAEHB and TAEHB (Dorman et al. 1993) are marked with "a" and "b", respectively. The HeMS is taken from Divine (1965) and Paczyński (1971a) and are marked with "c" and "d", respectively. Eddington luminosity fractions are also plotted with point-dashed lines and marked with the characteristic luminosities ($\log L/L_{\text{Edd}}$) in the cumulative luminosity distribution (Figure 4). He-rich ($\log(n\text{He}/n\text{H}) > -1$) stars are indicated with disks, He-poor ($\log(n\text{He}/n\text{H}) < -2.2$) with triangles and stars with $-2.2 < \log(n\text{He}/n\text{H}) < -1$

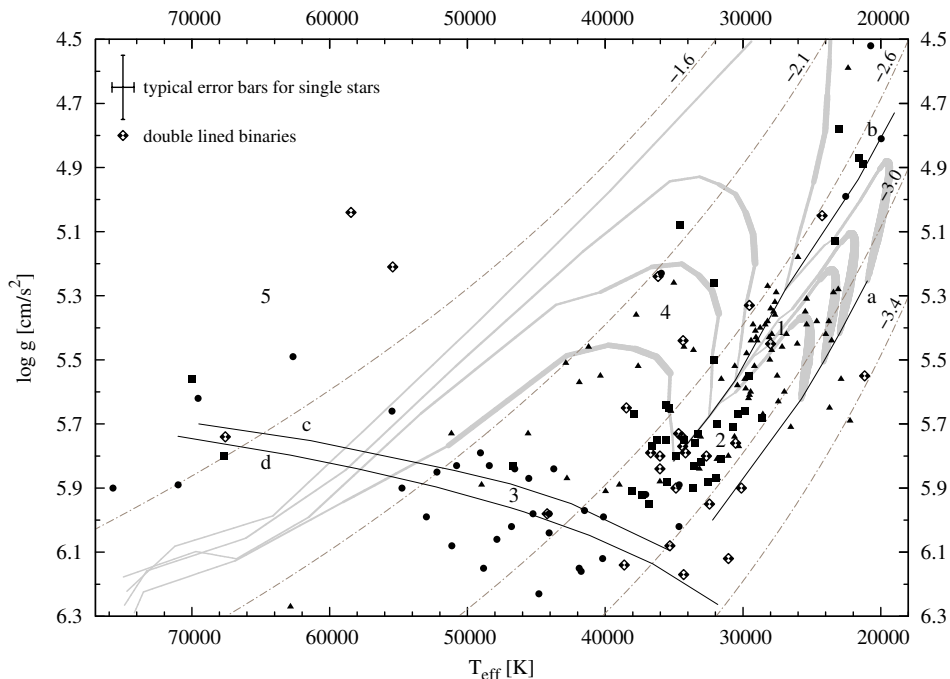


Figure 3. Sample of 181 hot stars on the $T_{\text{eff}}-\log g$ diagram. Typical error bars are shown in the upper left corner.

with squares. Subdwarfs in resolved composite spectra binaries are shown with diamonds. A correlation between surface temperature, gravity and He abundance can be immediately seen in Figure 3.

We distinguish five regions, marked from 1 to 5 in Figure 3. The cooler H-rich sdB stars (#1) are found around 28000 K and $\log g = 5.45$. Many of these are possible long-period pulsators ($P \sim 40-170$ min). The hotter sdB stars (#2) near 33500 K and $\log g = 5.8$ are on average ten times more He abundant and some can be short-period pulsators ($P \sim 2-6$ min). The hot He-sdO stars (#3) are found over 40000 K near $\log g = 6$. H-rich sdO stars (#4) are over the EHB and HeMS, and finally, the least defined population, possible white dwarfs (low mass WDs, post-AGB and CSPN stars) that cross this region in the HRD on their cooling tracks (#5). The known shift of EHB stars towards higher temperatures with respect to the theoretical EHB band (Heber 2009) and the lack of stars along sections of fast evolution are notable.

From the effective temperature and surface gravity, the luminosity as a fraction of the Eddington luminosity can be derived assuming pure electron scattering in fully ionized H atmospheres (Lisker et al. 2005). This fraction is independent of stellar mass and proved to be a useful tool in investigating sample completeness. Our cumulative luminosity distribution and probability density is shown in Figure 4. The change of slope in the cumulative luminosity function clearly marks the ZAEHB at $\log(L/L_{\text{Edd}}) = -3$, the TAEHB at $\log(L/L_{\text{Edd}}) = -2.6$ and when stars leave the post-EHB evolutionary phase (TAPEHB) near $\log(L/L_{\text{Edd}}) \sim -2.0$. A change in the slope of sdO stars distinguishes He-rich and He-weak sdO stars. A similar overlapping of two populations can be outlined for sdB stars as well. We found the luminosity distribution of our sample

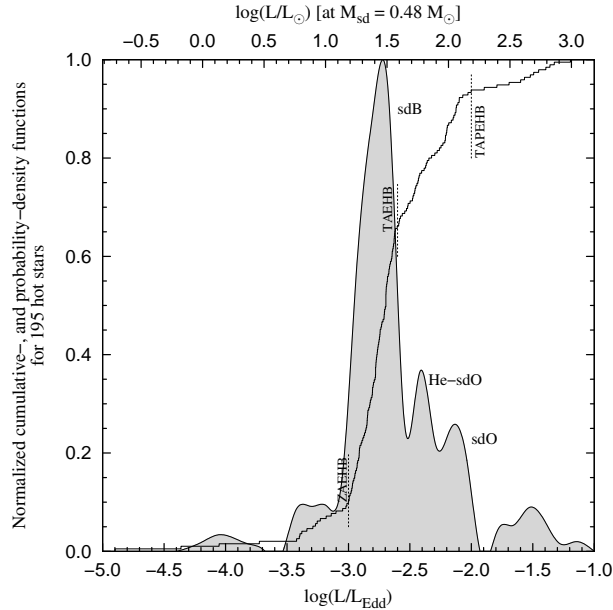


Figure 4. Luminosity distribution of 195 hot stars in the GALEX sample.

in good agreement with previous studies, e.g., the HS (Edelmann et al. 2003), the SPY sdB (Lisker et al. 2005) and the SPY sdO (Stroeer et al. 2007) surveys, and conclude that our sample is statistically complete.

4.2. The T_{eff} – He plane

The He abundance is another fundamental parameter of subdwarf stars that needs to be investigated along with effective temperature and surface gravity. Figure 5 shows the He abundance vs. effective temperature in our sample. The five groups defined in Section 4.1 are well represented and marked in the figure. The He-rich and He-weak sequences are clearly separated and show a similar trend with effective temperature. For the He-rich sequence we plot the best fit line from the HS sample (Edelmann et al. 2003) with short-dashed line in Figure 5. This independently derived trend fits our data as well. However, we found a completely different trend for the He-weak sequence, dash-dot line in Figure 5, possibly because the temperature range of the He-weak sequence was under-represented in the HS survey. The lack of stars around $\log(n\text{He}/n\text{H}) = -0.5$ over 40000 K can be seen just like the extreme He over-abundance of He-sdO stars around 40000 K. One star (*TYC 6017-419-1*) shows a pure He atmosphere and we could determine only a lower abundance limit. The recorded signal-to-noise of about 100 set our detection limit near $\log(n\text{He}/n\text{H}) = -3.5$.

4.3. CN abundance

Estimating metal abundances from optical spectra is more difficult because CNO is relatively unimportant in calculating the model atmosphere structure and the majority of their lines are in the UV. Out of the 181 stars, we measured a He abundance in 148

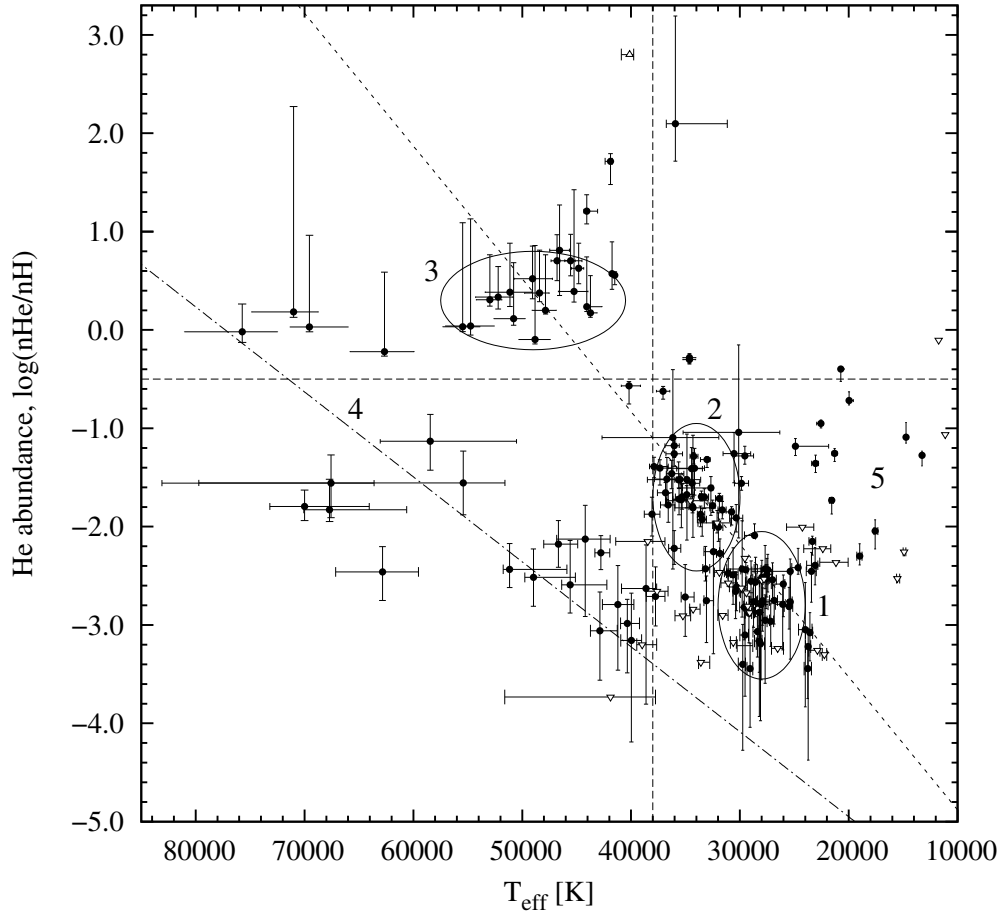


Figure 5. He abundance vs. effective temperature. Two trends showing increasing abundance with effective temperature can be seen. Also remarkable are the five marked groups introduced in Section 4.1. Upper limits are indicated with down open triangles.

objects, 67 showed N, and 35 showed measurable C abundance. There is a correlation between He, C and N abundances with a number ratio of about 400:1:2.

5. Conclusions

We have presented a subdwarf sample of 127 sdB and 40 sdO stars from the GALEX survey. Our selection provides a complete, homogeneously modelled sample of hot subdwarf stars, similar to the HS and SPY surveys. This high-quality set confirms well-known correlations between effective temperature and He abundance. A dichotomy seems to emerge for sdB stars that separates stars around 28000 K and $\log g = 5.45$ from stars near 33500 K and $\log g = 5.8$. This separation is seen in the He abundance pattern and its connection to binarity will be investigated further. The full catalogue, along with further details of spectral modelling, binary decomposition and on several individual stars will be presented in a forthcoming paper.

Acknowledgments. We acknowledge support from the Grant Agency of the Czech Republic (GA ČR P209/10/0967) and from the Grant Agency of the Academy of Sciences of the Czech Republic (IAA 300030908, IAA 301630901). Observations were made with ESO telescopes at the La Silla Paranal Observatory under programmes 82.D-0750, 83.D-0540, 85.D-0866 and with the NOAO Mayall telescope at the Kitt Peak National Observatory.

References

- Cenarro A. J., Peletier R. F., Sánchez-Blázquez P., Selam S. O., Toloba E., Cardiel N., Falcón-Barroso J., Gorgas J., Jiménez-Vicente J., Vazdekis A., 2007, *MNRAS*, 374, 664
- Divine N., 1965, *ApJ*, 142, 824
- Dorman B., Rood R. T., O’Connell R. W., 1993, *ApJ*, 419, 596
- Edelmann H., Heber U., Hagen H.-J., Lemke M., Dreizler S., Napiwotzki R., Engels D., 2003, *A&A*, 400, 939
- Geier S., Hirsch H., Tillich A., Maxted P. F. L., Bentley S. J., Østensen R. H., Heber U., Gänsicke B. T., Marsh T. R., Napiwotzki R., Barlow B. N., O’Toole S. J., 2011, *A&A*, 530, A28
- Han Z., Podsiadlowski Ph., Maxted P. F. L., Marsh T. R., Ivanova N., 2003, *MNRAS*, 336, 449
- Heber U., 2009, *Annu. Rev. A&A*, 47, 211
- Hubeny I., Lanz T., 1995, *ApJ*, 439, 875
- Kawka A., Vennes S., Nemeth P., Kraus M., Kubát J., 2010, *MNRAS*, 408, 992
- Lanz T., Hubeny I., 1995, *ApJ*, 439, 905
- Lanz T., Hubeny I., 2003, *ApJS*, 146, 417
- Lanz T., Hubeny I., 2007, *ApJS*, 169, 83
- Lisker T., Heber U., Napiwotzki R., Christlieb N., Han Z., Homeier D., Reimers D., 2005, *A&A*, 430, 223
- Napiwotzki R., Karl C. A., Lisker T., 2004, *Ap&SS*, 291, 321
- Østensen R. H., Oreiro R., Solheim J.-E., Heber U., Silvotti R., González-Pérez J. M., Ulla A., Pérez Hernández F., Rodríguez-López C., Telting J. H., 2010, *A&A*, 513, A6
- Paczyński B., 1971a, *Acta Astron.*, 21, 1
- Reed M. D., Stiening R., 2004, *APSS*, 291, 329
- Stroeer A., Heber U., Lisker T., Napiwotzki R., Dreizler S., Christlieb N., Reimers D., 2007, *A&A*, 462, 269
- Vennes S., Kawka A., Nemeth P., 2011, *MNRAS*, 410, 2095
- Vennes S., Thorstensen J. R., Kawka A., Németh P., Skinner J. N., Pigulski A., Stęślicki M., Kołaczowski Z., Śródka P., 2011, *ApJL*, 737, L16